Biosensors and Bioelectronics: X 2 (2019) 100026

Contents lists available at ScienceDirect

Biosensors and Bioelectronics: X

journal homepage: www.journals.elsevier.com/biosensors-and-bioelectronics-x

Fiber-based early diagnosis of venous thromboembolic disease by label-free D-dimer detection

Pablo Zubiate[a], Aitor Urrutia[a], Carlos R. Zamarreño[a,b], Josune Egea-Urra[c,d], Joaquín Fernández-Irigoyen[c,d], Ambra Giannetti[e], Francesco Baldini[e], Silvia Díaz[a,b], Ignacio R. Matias[a,b], Francisco J. Arregui[a,b], Enrique Santamaría[c,d], Francesco Chiavaioli[e,**], Ignacio Del Villar[a,b,*]

[a] Electrical and Electronic Engineering Department, Public University of Navarra, 31006, Pamplona, Spain
[b] Institute of Smart Cities (ISC), Public University of Navarra, 31006, Pamplona, Spain
[c] Clinical Neuro proteomics Group, Navarrabiomed, Complejo Hospitalario de Navarra (CHN), Universidad Pública de Navarra (UPNA), IdiSNA, Irunlarrea, 31008, Pamplona, Spain
[d] Proteored-ISCIII. Proteomics Unit, Navarrabiomed, Complejo Hospitalario de Navarra (CHN), Universidad Pública de Navarra (UPNA), IdiSNA, Irunlarrea, 31008, Pamplona, Spain
[e] Institute of Applied Physics "Nello Carrara" (IFAC), National Research Council of Italy (CNR), 50019, Sesto Fiorentino, Italy

ARTICLE INFO

Keywords:
Optical biosensor
Lossy mode resonance
D-dimer
Venous thromboembolism
Nanocoated fiber

ABSTRACT

D-dimer is a useful diagnostic biomarker for deep vein thrombosis or pulmonary embolism, collectively referred to as venous thromboembolism (VTE). The ability to detect in real-time the amount of D-dimer with a fast and reliable method is a key step to anticipate the appearance of these diseases. Here, the results of a highly specific and sensitive biosensor for the detection of D-dimer based on lossy mode resonance in fiber optics are presented. The unique features of specialty fibers in light management integrated with microfluidics allow detecting D-dimer in human serum with a detection limit of 100 ng/mL, a value 5-fold below the clinical cutoff value. Comparison of the results achieved with mass-spectrometry-based proteomics, which allows for the identification of beta- and gamma-chains of fibrinogen, demonstrates the ability of our platform to specifically (>90%) recognize D-dimer. Therefore, this technology potentially represents a paradigm shift in the development of a simple, high-specificity and label-free biosensing platform, which can be applied to speed up diagnostic healthcare processes of venous thromboembolism toward an early diagnostic and personalized treatment system.

1. Introduction

D-dimer antigen, the smallest product originated from cross-linked fibrin degradation, is used, above a cutoff value, as a biomarker for deep vein thrombosis or pulmonary embolism, collectively referred to as venous thromboembolism (VTE) (Adam et al., 2009; Kogan et al., 2016). About 10 million cases of VTE occur every year, thereby representing the third leading vascular disease after acute myocardial infarction and stroke (Raskob et al., 2014), and the diagnostic work-up of suspected VTE includes the sequential application of a clinical decision rule and D-dimer testing (Di Nisio et al., 2016). Recently, D-dimer assays are routinely used to predict which patients are more likely to suffer recurrent thrombosis when anticoagulant treatments are stopped (Linkins and Takach Lapner, 2017).

Moreover, D-dimer can also be used as a predictive value for major adverse cardiovascular events (MACE) and non-coronary artery bypass grafting (non-CABG) major bleeding (Kikkert et al., 2014). However, despite the importance of D-dimer monitoring by the clinicians, D-dimer assays are highly variable, depending on the method of capture and on the instrumentation used (Longstaff et al., 2016; Olson et al., 2013; Spannagl et al., 2005). The clinical cutoff value of D-dimer is 0.5 μg/mL (manufacturer's recommended threshold for STA®-Liatest® D-di; Stago, Asnières sur Seine Cedex, France) (Linkins and Takach Lapner, 2017; Marill, 2008; Weitz et al., 2017). This value is used, once exceeded, as a screening tool for acute aortic dissection (Shimony et al., 2011), and the sensitivity and specificity of D-dimer above this cutoff value for cardioembolic subtype are 78% and 79%, respectively (Bernard et al., 2010). Therefore, it turns out obvious that measuring

* Corresponding author. Electrical and Electronic Engineering Department, Public University of Navarra, 31006, Pamplona, Spain.
** Corresponding author.
E-mail addresses: f.chiavaioli@ifac.cnr.it (F. Chiavaioli), ignacio.delvillar@unavarra.es (I. Del Villar).

https://doi.org/10.1016/j.biosx.2019.100026
Received 22 May 2019; Received in revised form 23 July 2019; Accepted 8 August 2019
Available online 21 August 2019

and controlling the amount of D-dimer is critical for preventing some important diseases. As reported in (Di Nisio et al., 2007), taking into account more than 300 D-dimer test evaluations described in 184 different articles, enzyme-linked immunosorbent assays (ELISA), enzyme-linked fluorescent assays (ELFA) and quantitative latex agglutination assays (QLAA) were more sensitive than whole-blood agglutination assays. Therefore, the whole-blood D-dimer assay should not be used (Weitz et al., 2017). In addition to this, despite there are few works on sensors for D-dimer detection (Bourigua et al., 2010; Chebil et al., 2010; Gao et al., 2015; Grant; Glass, 1999; Koukouvinos et al., 2016), none of them makes use of a label-free detection approach where the interaction of D-dimer with the sensing surface is monitored in real time.

Fiber optics, the best platform for communications and light management, is a good candidate to address the challenge and, at the same time, features unique peculiarities such as small size, lightweight, immunity to electromagnetic interferences and utilization in harsh environments. However, it is sometimes discarded in biosensing because of its low sensitivity.

During the last years, much progress has been done towards improving this characteristic. Different sensing mechanisms and geometries have been explored (fiber Bragg gratings, interferometers, photonic crystal fiber, or microstructured fibers) (Liu et al., 2018; Wu et al., 2009), which allow obtaining devices with improved properties and performances that can be considered as a lab-on-fiber (Principe et al., 2017). The combination of the previous geometries with the nanodeposition of a thin-film has increased even more the domains of application and the potential of optical fibers (Caucheteur et al., 2016; Chiavaioli et al., 2017a; Stern et al., 2017). Not only the deposition of a nanocoating sensitive to a specific parameter turns the optical fiber into an environmental sensor, a chemical sensor or a biosensor, but also the nanocoating can be used as an element that increases the inherent sensitivity of the device. As an example, with the mode transition phenomenon it is possible to enhance the sensitivity in long period gratings (LPGs) and single-mode multimode single-mode (SMS) fiber configuration by more than one order of magnitude (Cusano et al., 2006; Del Villar et al., 2005). In other cases, the nanocoating is responsible for the generation of resonances related to physical phenomena such as surface plasmon resonance (SPR) (Gramotnev and Bozhevolnyi, 2010; Hoa et al., 2007; Homola, 2008) or lossy mode resonance (LMR) (Kosiel et al., 2018; Paliwal and John, 2015; Tiwari et al., 2017), whose the spectral shift of the resonance is used as a parameter to detect changes in the thin-film itself or in the subsequent deposition of additional layers.

Despite LMRs are not as well known as SPRs, they possess very interesting features, such as the possibility to tune the position of the resonance at any wavelength in the optical spectrum from the visible to NIR, just by controlling the thickness of the nanocoating, and the opportunity to use alternative materials (i.e. polymers and metallic oxides) to the metallic ones used for SPRs (Del Villar et al., 2017). Moreover, by means of the combination of the deposition of nanometric thin-films that generate LMRs with exotic fiber geometries, such as D-shaped fibers, it is possible to obtain sensitivities of more than 1×10^6 nm per refractive index unit (nm/RIU) in the silica region (1.45 RIU) and of more than 1.4×10^4 nm/RIU in the water region (1.33 RIU) (Arregui et al., 2016). Since the sensitivity to refractive index (RI) is often used as a test for the prediction of the device performance, these values indicate the potential of this type of devices when used as a biosensor. Based on this approach, it has been possible to detect immunoglobulin G at femtomolar concentration in human serum (Chiavaioli et al., 2018).

In the present paper, we describe a simple, high-specificity and label-free LMR-based biosensing platform consisting of a nanocoated D-shaped fiber for the real-time monitoring of D-dimer, which is a key advance towards theranostic treatments of VTE for personalized medicine. Thanks to the very sensitive approach integrated with microfluidics, a detection limit of 100 ng/mL (500 pM) was achieved in human serum, a value 5-fold below the clinical cutoff value. Comparison of the results achieved with mass-spectrometry-based proteomics, which was used to prove the grafting of D-dimer to the fiber surface through peptide sequencing and bioinformatics protein identification, also demonstrates the ability of the proposed platform to specifically (> 90%) recognize D-dimer in diluted and undiluted biological matrices and its reliability.

2. Materials and methods

2.1. Reagents

1-ethyl-3-(3-dimethylaminopropyl)carbodiimide hydrochloride (EDC) and N-hydroxysuccinimide (NHS) were purchased from Thermo Fisher Scientific. The methacrylic acid/methacrylate copolymer (Eudragit® L100) was purchased from Evonik Health Care. Ethanol (EtOH), phosphate-buffered saline (40 mM PBS, pH 7.4), bovine serum albumin (BSA) and the human D-dimer protein were purchased from Sigma Aldrich Inc. The corresponding high-affinity D-dimer antibody (Monoclonal mouse antibody, anti-D-dimer DD2), C-reactive protein and human serum were purchased from HyTest Ltd. Electrophoresis reagents were purchased from Bio-Rad: Urea (GE Healthcare Life Science), thiourea (GE Healthcare Life Science), and DTT (Acròs Organics), and trypsin from Promega.

2.2. Optical sensing and microfluidic system

The proposed optical sensing system is based on the lossy mode resonance, a technology based on enhancement of the evanescent field of the modes guided in the optical fiber due to the guidance of a mode in a nanometric thin-film whose real part of the RI is higher than that of the fiber substrate and whose imaginary part is low but not negligible (Del Villar et al., 2017). With a side polished (D-shaped) optical fiber, the width of the LMR resonance generated in the optical spectrum is reduced to such a point that this allows for an accurate measurement of the wavelength shift caused by changes in the outer medium (i.e. the modification of the surrounding RI or the deposition of an overlay material (Arregui et al., 2016)). In addition, the sensitivity of LMR-based devices is improved if the RI of the material deposited on the fiber is as high as possible (Del Villar et al., 2012). In a previous work, it was demonstrated with a similar structure, i.e. a cladding removed multimode fiber, that the use of SnO_{2-x} as coating material is better than ITO, since better performances were attained in terms of both refractive index sensitivity (Table 1) and limit of detection (Chiavaioli et al., 2018). The ellipsometric measurements confirmed the theory that a higher refractive index (real part) leads to a better sensitivity: in the used wavelength range, ranging from 1250 nm to 1750 nm, the refractive index of SnO_{2-x} is roughly 1.9, whereas it is 1.83 for ITO. In addition, it was also shown that the optical platform is critical for the performance of the biosensing system: if a D-shaped fiber is used instead of a cladding removed multimode fiber, the LOD can be improved by three orders of magnitude. This justifies the selection of SnO_{2-x} as coating material together with a D-shaped fiber. Amorphous silicon, IGZO and ZnO have also been explored with D-shaped fibers (Andreev et al., 2005, 2008; Ozcariz et al., 2019), but they showed sensitivities

Table 1
Sensitivity to refractive index changes of different materials generating lossy mode resonance.

Material	RI range	Sensitivity	Reference
IGZO	1.370–1.385	6700 nm/RIU	Ozcariz et al. (2019)
Amorphous silicon	1.33–1.38	5300 nm/RIU	Andreev et al. (2005)
ZnO	1.333–1.362	6700 nm/RIU	Andreev et al. (2008)
ITO	1.365–1.380	7800 nm/RIU	Zubiate et al. (2015)
SnO_{2-x}	1.321–1.326	14500 nm/RIU	Arregui et al. (2016)

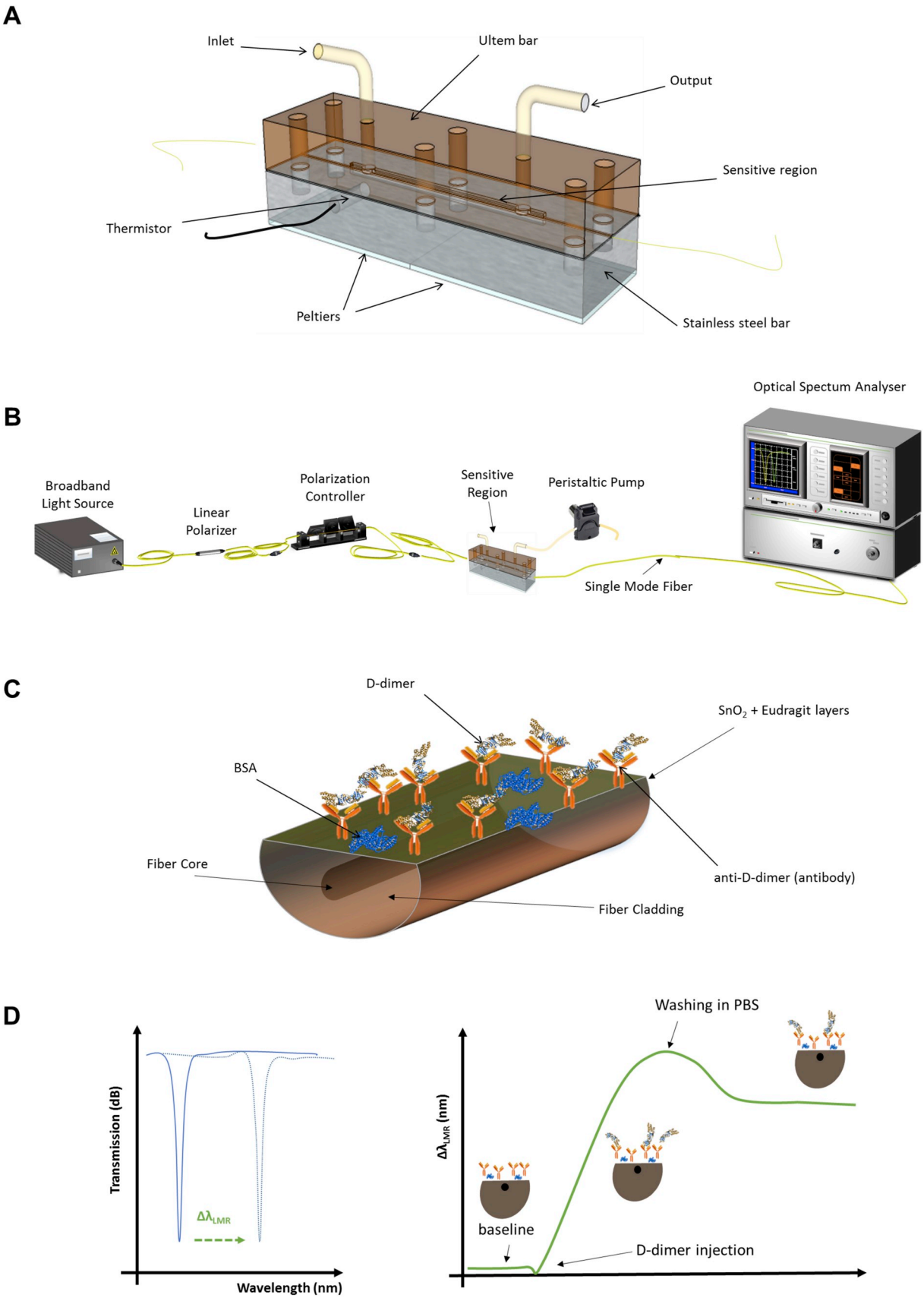

Fig. 1. Experimental setup, biosensing device and principle. (A) Detailed microfluidic system and flow channel with the temperature-stabilization system. (B) The entire experimental setup to monitor in real time the antibody immobilization and the interaction with the D-dimer. (C) Sketch of the proposed D-shaped fiber biosensor based on a lossy mode resonance approach. (D) A general diagram of the sensing principle and of the LMR wavelength shift corresponding to the D-dimer capture and the subsequent washing.

that are at least similar or lower than ITO (Table 1). Moreover, even though a material with a higher sensitivity is used, its performance in a microfluidic system should be tested. Therefore, the stability of ITO and SnO_{2-x} was compared in fluidic conditions. Unlike SnO_{2-x}, ITO experienced some drifts, which reinforced the idea of using SnO_{2-x} instead of ITO (Del Villar et al., 2019).

In order to obtain the D-shaped fiber configuration, standard single mode fibers (Corning SMF-28) with a cladding/core diameter of 125/8.2 μm are used. 17 mm of the fiber are progressively polished down until an attenuation of 1 dB at 1550 nm is attained in high RI matching oil (1.5 RIU).

Concerning the procedure of coating deposition of the SnO_{2-x} thin film, the D-shaped fiber is placed inside a DC sputter machine (K675XD from Quorum Technologies) at a partial pressure of argon of 9×10^{-2} mbar and an intensity of 90 mA, and a coating of around (160 ± 10) nm was deposited, according to (Chiavaioli et al., 2018).

After the deposition process, the fiber sensor is located inside a thermo-stabilized microfluidic system (Chiavaioli et al., 2014). The flow cell allows for control and manipulation of small volumes of liquid samples as well as temperature stabilization. As shown in Fig. 1A, the microfluidic system consists of two equal-size pieces (23 mm wide, 10 mm deep and 100 mm long), which can be assembled and sealed with Parafilm R® sheet interposed between the two parts in order to assure the water-proofing. The upper one is made of polyetherimide (ULTEM resin) and the bottom one is made of stainless steel. A microfluidic channel is fabricated on both bars with the size of 1 mm × 1 mm × 50 mm, thus attaining a volume of 50 μL, which perfectly fits the handling of small liquid samples. An inlet and an outlet are punched at both sides of the ULTEM piece. In addition, a v-groove of 0.5 mm deep is engraved on both ends of the stainless steel bar in order to house the fiber sensor, which is finally glued with its jacket to the v-groove edges using an UV optical flexible adhesive (Norland), allowing for the mechanical stabilization of the device. The stainless steel bar of the flow cell is heated with two Peltier cells (23 mm × 25 mm), whereas a thermistor is inserted into a lateral hole in the stainless steel bar, as shown in Fig. 1A. A temperature control system acquires the temperature from the thermistor and drives current to the Peltier cell in order to adjust the temperature at 30 °C (± 0.05 °C). Finally, the microfluidic system is connected to a peristaltic pump by means of a premium medical grade thermoplastic elastomer PHI tube, making it possible to pump the appropriate solution into the flow cell. The flow rate of each solution varies according to the biological procedure as detailed in the next section, devoted to the explanation of the surface functionalization and assay protocol.

The optical spectrum is monitored and recorded from the first phase of thin-film deposition up to the further biological stages (immobilization and detection) using the experimental setup depicted in Fig. 1B. A multi-LED light source (HP-83437A) is used as the optical source that launches light into the optical fiber. In order to control the polarization state of light, a fiber optics in-line polarizer and a polarization controller are located between the optical source and the D-shaped fiber sensitive region. Once light passes through the fiber, an optical spectrum analyzer (OSA, HP-86142A) collects the optical spectrum and allows the measurement of the LMR resonance wavelength.

2.3. Surface functionalization and assay protocol

The sketch of the biosensor is displayed in Fig. 1C. As a first step, the D-shaped fiber surface is coated with SnO_{2-x}. After that, the antibody is grafted on the sensor surface, according to the following steps:

i) the sensitive region of the fiber is immersed in 2 mM (0.04% w/v) Eudragit L100 copolymer in ethanol for 1 min and then is left drying in air for about 15 min until the solvent has completely evaporated. Eudragit L100 provides the free functionalities, i.e. carboxylic functional groups, necessary for the antibody immobilization on the sensor surface;
ii) the carboxylic groups are activated by means of an EDC/NHS solution (2 mM/5 mM, respectively), which is injected and flowed over the Eudragit at 14 μL/min when the sensor is safely placed inside the microfluidic system;
iii) immediate covalent immobilization of the antibodies on the activated surface is carried out, by injecting a solution of 500 μg/mL anti-D-dimer in PBS for 1 h at a flow rate of 7 μL/min;
iv) washing with PBS buffer is performed for 5 min at a flow rate of 20 μL/min, so as to remove the unreacted antibodies;
v) surface passivation with 1% (w/v) BSA in PBS is implemented: BSA is injected for 15 min at 14 μL/min to block unreacted remaining active carboxylic groups and to prevent non-specific adsorption on to the sensing surface.

Once the anti-D-dimer receptor is grafted on the fiber, the assay is completed by injecting different solutions of D-dimer protein at increasing concentrations that range from 0.1 μg/mL up to 100 μg/mL for 15 min each at a flow rate of 7 μL/min. A washing step with PBS is carried out for 5 min at 20 μL/min between each D-dimer protein solution injection in order to measure the surface effect due to the receptor-analyte binding interaction and, hence, to discard any volume effect related to the solution refractive index (Chiavaioli et al., 2017b). Fig. 1D accounts for a general diagram of the sensing principle and of the LMR wavelength shift corresponding to the D-dimer capture and the subsequent washing.

Specificity is confirmed in the first experiments by injecting a C-reactive protein, which is another biomarker for heart diseases like stroke, while in the other experiments the same model assay is also performed in human serum diluted 1:10 (v/v) in PBS and undiluted serum, by spiking D-dimer protein at different concentrations.

The biological steps are carried out within the microfluidic system, keeping the external temperature as stable as possible at (25 ± 1) °C and the flow cell temperature at (30 ± 0.05) °C. This temperature has been chosen in order to avoid the oscillations of the temperature control system described in the previous section. In fact, it turns out that a slightly different temperature with respect to that of the environment has to be selected to make the temperature as stable as possible for long-term measurements. All the binding interactions are performed *in situ*, and are continuously monitored in real time through the experimental setup of Fig. 1B.

2.4. Gel electrophoresis and immunoblotting

As purity analysis concerns, protein denaturation from the sensing surface of the fiber is firstly performed by applying a lysis buffer containing urea (7M), thiourea (2M) and DTT (0.5%) for 5 min at 95 °C. Afterwards, protein content is let it precipitate by acetone 0/N at −20 °C. Later, both D-dimer protein and DD2 anti-D-dimer antibody (1–5 μg) are re-suspended in 4x Laemmli buffer in the presence of beta-mercaptoethanol. After that, the biomolecules are separated by sodium dodecyl sulphate-polyacrylamide gel electrophoresis (12.5% acrylamide).

For specificity analysis, DD2 anti-D-dimer antibody were used to detect potential D-dimer products by Western-blotting using the procedure described in (Lachén-Montes et al., 2017). Briefly, D-dimer protein is re-solved in 12.5% acrylamide gels and electrophoretically transferred onto nitrocellulose membranes using a Trans-blot Turbo transfer system in 7 min (up to 25 V). Membranes are then probed with the antibody at 1:1000 dilution in 5% non-fat milk. After incubation with the appropriate horseradish peroxidase-conjugated secondary antibody (1:5000 dilution), the immunoreactivity is visualized by enhanced chemiluminiscence (PerkinElmer) using a Chemidoc MP Imaging System (Bio-Rad). Finally, densitometric analysis is performed with the Image Lab tool (Software Version 5.2).

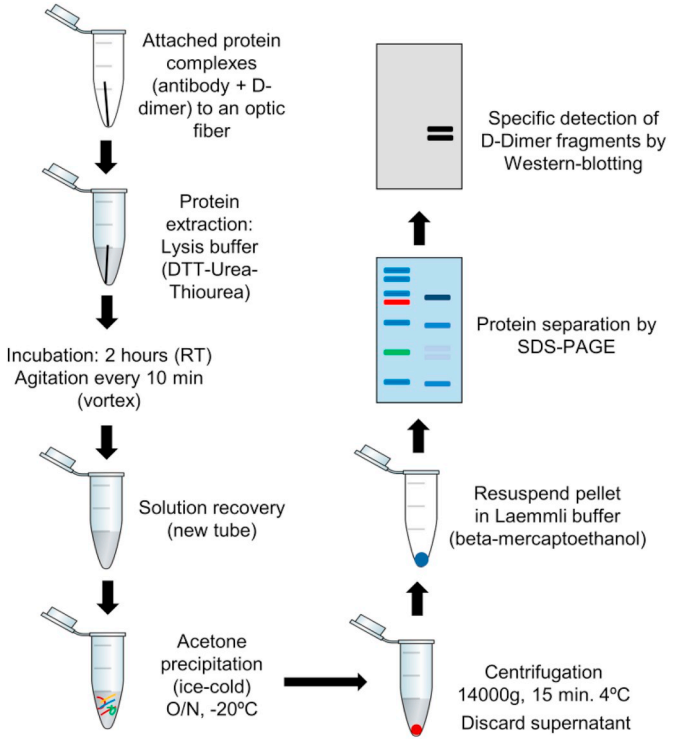

Fig. 2. Technical workflow used to verify the binding of D-dimer onto the functionalized biosensor surface. Detachment of D-dimer protein from the functionalized fiber surface possessing the BRE, its separation through Sodium Dodecyl Sulphate-PolyAcrylamide Gel Electrophoresis (SDS-PAGE) and, finally, its detection by Western-blotting (W-b).

The entire previously described technical workflow, which is used to verify the binding of D-dimer onto the functionalized biosensor surface, is sketched step-by-step in Fig. 2.

2.5. Protein identification by mass spectrometry

D-dimer (3 µg) is diluted in 4x Laemmli buffer and loaded into a 0.75 mm thick polyacrylamide (12.5%) resolving gel. Bands are stained with Coomassie Brilliant Blue staining and excised from the gel. Protein enzymatic cleavage is carried out with trypsin (1:20, w/w) for 16 h at 37 °C using the procedure described in (Shevchenko et al., 2007). Peptides mixtures are separated by reverse phase chromatography using a NanoLC-Ultra 2D pump system (Eksigent) fitted with a 75 µm ID column (0.075 × 250, Eksigent). During the process, pre-column is in line with column and flow is maintained all along the gradient at 300 nL/min. Eluting peptides from the column are analyzed using a Sciex 5600 Triple-TOF system. Tandem MS/MS data acquisition and protein identification are performed using the procedure described in (Lachén-Montes et al., 2017; Socorro et al., 2017).

3. Results

The LMR generated with the deposition of a nanometric film of conductive black tin oxide, SnO_{2-x}, on D-shaped fibers is used to detect D-dimer/anti-D-dimer interactions. The operation principle consists of monitoring in real time the interaction between a protein (D-dimer) and the specific antibody (anti-D-dimer) - the so-called capture antibody - grafted on the D-shaped fiber, which induces changes in the thickness of the coating and in the effective RI of the sensing layer. An accurate determination of this change can be attained by detecting the wavelength shift of the LMR (λ_{LMR}).

3.1. Detection of Human D-dimer in buffer

In order to demonstrate the ability of the nanometric film coated D-shaped fiber-based biosensor for a label-free detection of D-dimer in PBS buffer (pH 7.4), its response to different concentrations of D-dimer protein was analyzed. The capture immobilization, the first part of any assay protocol, plays an important role in terms of development of the proposed biosensor. In addition, as it is indicated in Methods section, monoclonal anti-D-dimer antibodies were selected as biological recognition element (BRE) due to their high affinity and specificity with D-dimer protein. The results related to this first part of the model assay, step-by-step described in Methods section, are detailed in Supplementary Fig. 1. The transmission spectrum of the sensor was monitored during the entire experiment and the wavelength shift of the LMR was tracked in real time in order to achieve the sensorgram. Fig. 3A shows the sensorgram of D-shaped fiber biosensor during the injection of D-dimer protein at increasing concentrations. The sensorgram displays the signal change, compared to the baseline, to D-dimer solutions ranging from 0.1 µg/mL up to 100 µg/mL. Here, it can be seen that the LMR wavelength changes with the concentration of D-dimer or, in other words, the LMR wavelength shifts toward longer wavelengths as the concentration of D-dimer increases. As in all label-free biosensors, after the injection of the target analyte at different concentrations, and the subsequent attainment of a stationary equilibrium, a washing step with PBS is performed in order to remove all the unbound D-dimer. Therefore, the wavelength shift after the washing step with respect to the signal value before the D-dimer solution injection is only related to the amount of D-dimer captured by the specific receptor grafted on the fiber surface and can be directly associated to the D-dimer concentration.

Fig. 3B accounts for the calibration curve of the biosensor, which represents the shift of the LMR wavelength as a function of the concentration of D-dimer protein. As an additional parameter for performance assessment among the biosensors tested, the relative shift of λ_{LMR} (normalized by the initial value of λ_{LMR}) is detailed in Supplementary Fig. 2. The value of each experimental point was obtained by averaging over 15–20 distinct measurements at flow stopped after each washing step in buffer. As shown in Fig. 3B, the response of the device exhibits the typical sigmoidal behavior without reaching the highest values (upper asymptote) where the saturation of the biosensing layer is obtained, because small concentrations of D-dimer have been explored. The experimental points are fitted by the Hill function with a R^2 regression coefficient of 0.9968. The Hill equation, which is formally equivalent to the Langmuir isotherm, is a well-accepted mathematical model that provides a way in which to quantify the degree of interaction between ligand binding sites (Gesztelyi et al., 2012). A total wavelength shift of 16.78 nm for D-dimer concentrations varying from the baseline to 100 µg/mL is achieved. From the calibration curve of Fig. 3B, it is possible to extrapolate the limit of detection (LOD) of the biosensor, defined as the signal of the blank plus three times the standard deviation of the blank (Shrivastava and Gupta, 2011). For the sake of simplicity, the LMR wavelength has been scaled down at 0 nm in each calibration curve, therefore LODs have been calculated as three times the standard deviation of the blank (Chiavaioli et al., 2017b). By looking the detail of the inset of Fig. 3B, the LOD for the proposed biosensor is 10 ng/mL (50 pM), considering σ_{blank} = 16.8 pM (picometer). Moreover, it should be pointed out that the error bars correspond to the measurements of four identical and independent sensors (n = 4) in order to assess the repeatability and reproducibility of the proposed biosensor. The LMR device details a response to D-dimer in PBS in the concentration range of 0.1–100 µg/mL. The minimum shift of resonant wavelength is 0.232 nm at 0.1 µg/mL, whereas the maximum shift is 16.78 nm at 100 µg/mL. In addition, in order to provide a more realistic and reliable assessment of the biosensor performance, the limit of quantification (LOQ) is also evaluated by defining it as the signal of the blank plus ten times the standard

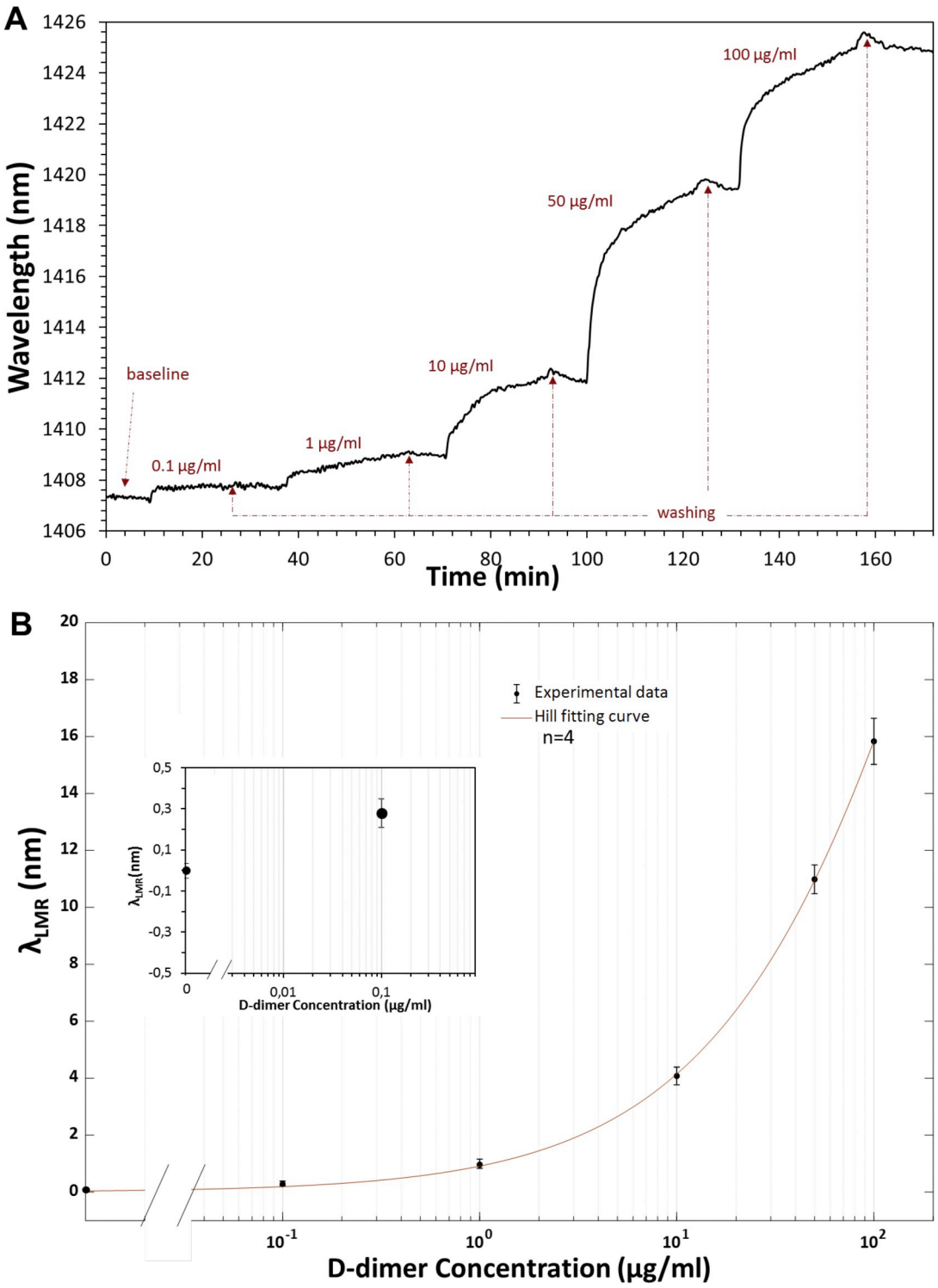

Fig. 3. Detection of Human D-dimer protein in PBS. (A) Sensorgram of D-shaped fiber biosensor during injection of increasing concentrations of D-dimer. All the analyte concentrations from baseline up to 100 µg/mL are displayed, with a total shift of the λ_{LMR} of 16.78 nm. (B) Calibration curve of four identical and independent biosensors (n = 4) detecting D-dimer in PBS with the Hill fitting curve of the experimental points. The inset details the wavelength shift and error bar of the blank and first D-dimer concentrations.

deviation of the blank (Shrivastava and Gupta, 2011). The LOQ for the proposed biosensor is 80 ng/mL (400 pM).

In order to study the specificity of the biosensors, they are exposed to different solutions of D-dimer spiked with a non-specific protein, C-reactive protein (CRP). The results, which are detailed in Supplementary Fig. 3, clearly show a flat response during the injection of CRP at 30 µg/mL, which demonstrates a biosensor specificity greater than 90%. Moreover, the shift of LMR wavelength related to the injection of a solution of 10 µg/mL D-dimer and 10 µg/mL CRP and the subsequent washing in PBS is roughly 4 nm, perfectly comparable with that shown in Fig. 3. The same can be said about the 8 nm shift attained with 30 µg/mL D-dimer and 50 µg/mL CRP. This testifies again the biosensor specificity and corroborates that the shift of λ_{LMR} is directly associated with the interaction of the D-dimer protein.

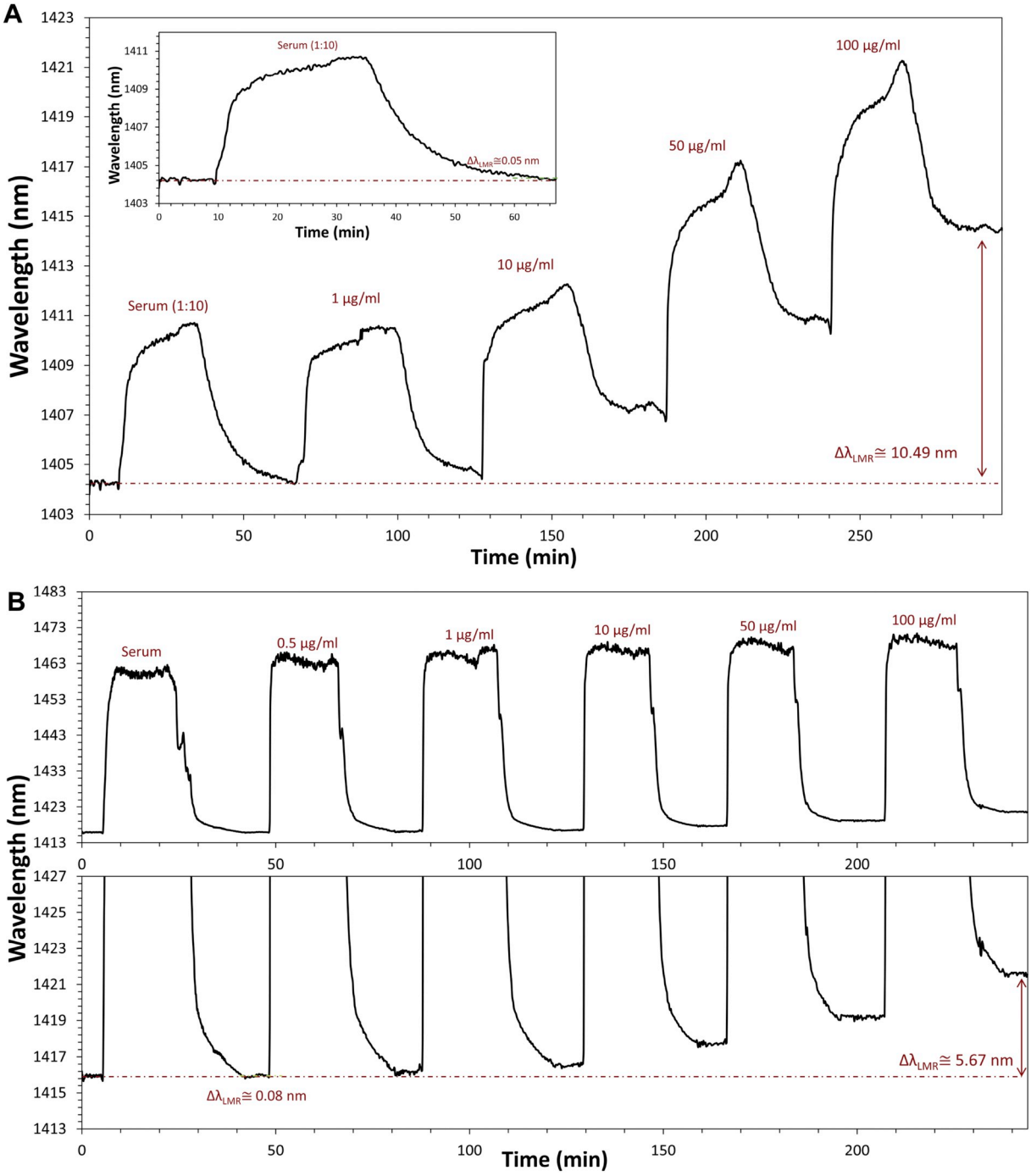

Fig. 4. Detection of Human D-dimer protein in human serum. (A) Sensorgram of D-shaped fiber biosensor during injection of increasing concentrations of D-dimer (range 1–100 µg/mL) spiked with serum diluted in PBS (1:10). Inset: specificity test representing the signal change, i.e. the LMR wavelength shift, in PBS after the injection of serum without the specific analyte under investigation (D-dimer). (B) Sensorgram of D-shaped fiber biosensor during injection of increasing concentrations of D-dimer (range 0.5–100 µg/mL) spiked with undiluted serum (top chart). Bottom chart: zoom of the previous sensorgram showing the change of the signal of interest taken in PBS at flow stopped.

3.2. Detection of Human D-dimer in human serum

The next step is the implementation of the assay using human serum samples, in order to investigate the application of the biosensor much closer to the real situation toward clinical applications. In the same way, the binding between the antibody and the protein is monitored in real time during the implementation of the same assay with the D-dimer spiked in human serum. Two different assays are performed, one with the serum diluted in PBS (1:10) and the other with undiluted serum. Fig. 4A details the sensorgram of a D-shaped fiber biosensor in the first case, while Fig. 4B in the second case. It should be pointed out that the background wavelength shift experienced in both diluted and undiluted serums is due to refractive index of the solution in which the D-dimer is spiked. All the refractive index-based optical sensors are sensitive not only to the adhesion of molecules on the sensor surface (surface refractive index change), but also to the refractive index of the surrounding medium (volume refractive index change). Both contribute to the background wavelength shift, even if the second effect can be considered almost instant when the solution enters the microfluidic system (Chiavaioli et al., 2017b). It turns out that the background

wavelength shift in the sensorgram achieved with undiluted serum (Fig. 4B) is larger than in diluted serum (Fig. 4A) because the refractive index of undiluted serum is higher than that of diluted serum. As described in section 2.3, since all the experimental points in the calibration curves are taken at flow stopped after the washing in PBS buffer, there is no contribution of the (diluted and undiluted) serum refractive index in the results, thus all the LMR wavelength shifts will be only due to adhesion of D-dimer onto the biosensing layer.

In addition, the inset of Fig. 4A shows the specificity test representing the shift of λ_{LMR} in PBS after injection of serum only, without the specific analyte under test (D-dimer). This shift, taken in PBS before (baseline) and after the injection of serum, was (0.05 ± 0.02) nm, whereas a larger shift is observed in the successive steps when D-dimer is spiked with serum, indicating that the protein interacted with the capture antibody with a specificity >90%. The same can be asserted in the case of undiluted serum (Fig. 4B) with a shift of LMR wavelength of (0.08 ± 0.025) nm and a specificity >80%.

Fig. 4 reports on the total wavelength shift of 10.49 nm and of 5.67 nm obtained with the two assays in the case of diluted and undiluted serums, respectively. In the second case, the total shift is almost half of the first case and this can be explained considering a greater difficulty and, hence, a less probability for the analyte to reach the receptor due to a denser matrix and/or to a more intense electric charge effect over the biomolecules (Squires et al., 2008). Moreover, the effect of volume RI change is evident in Fig. 4B if the signal in serum and in PBS is compared. In fact, the signal change is so big that a zoom of the interested part is presented to see the signal change in PBS after the injection of D-dimer solutions in serum and the successive washing. However, it is worth pointing out that this does not affect the capability of the biosensor to detect D-dimer at very low concentrations.

Fig. 5 accounts for the calibration curve of the two biosensors when the assays have been performed with diluted (green symbols) and undiluted (blue symbols) serums. The value of each experimental point is obtained by averaging over 15–20 distinct measurements at flow stopped after each washing step in PBS as detailed in Methods section. In these cases, no repeated experiments have been performed ($n = 1$). Consequently, in this second case of Fig. 5, the error bars referred just to the above-mentioned procedure.

The LOD for the proposed biosensor is 100 ng/mL (0.5 nM) in the case of diluted serum, considering σ_{blank} = 34 pM (picometer), while it is a bit higher, 320 ng/mL (1.6 nM), in the case of undiluted serum for the same reasons discussed previously. In any case, the usual protocol in clinical applications concerning human samples is to apply a dilution (1:5 or 1:10) to avoid any matrix effect (Zhang et al., 2014). However, the results of Fig. 5 detail clearly the ability of the biosensor to properly work with undiluted human serum. Moreover, the LOQs for the biosensors implemented in human diluted and undiluted serums are 800 ng/mL (4 nM) and 2.4 μg/mL (12 nM), respectively. Even if the LOQs are higher than the clinical cutoff value, in the case of diluted serum we are very close to it (800 ng/mL against 500 ng/mL) which makes us confident that a slight optimization in the optical platform will allow us the achievement of this objective also considering that the LOD is 5-fold below the clinical cutoff value.

3.3. Evidence of human D-dimer binding onto the functionalized biosensor surface

As a further evidence, in order to verify the binding of D-dimer onto the functionalized biosensor surface having the BRE, a technical workflow has been developed. It consists of the detachment of D-dimer protein, then of its separation through Sodium Dodecyl Sulphate-PolyAcrylamide Gel Electrophoresis (SDS-PAGE) and, finally, of its detection by Western-blotting (W-b). All the steps are detailed in Methods section. Fig. 6A shows the results of D-dimer separation by SDS-PAGE using the Ponceau staining, whereas Fig. 6B details the results obtained with W-b. It turns out that Ponceau staining is not sensitive enough to detect the presence of D-dimer protein, but is useful because it does not appear to have a deleterious effect on the sequencing of blotted biomolecules and, hence, is the selected method for locating them through W-b. In fact, W-b reveals a specific band of protein detached from the fiber biosensor placed between 25 and 35 kDa (Fig. 6B).

In order to characterize the protein band previously obtained, mass spectrometry is used to identify the presence of D-dimer. The procedure

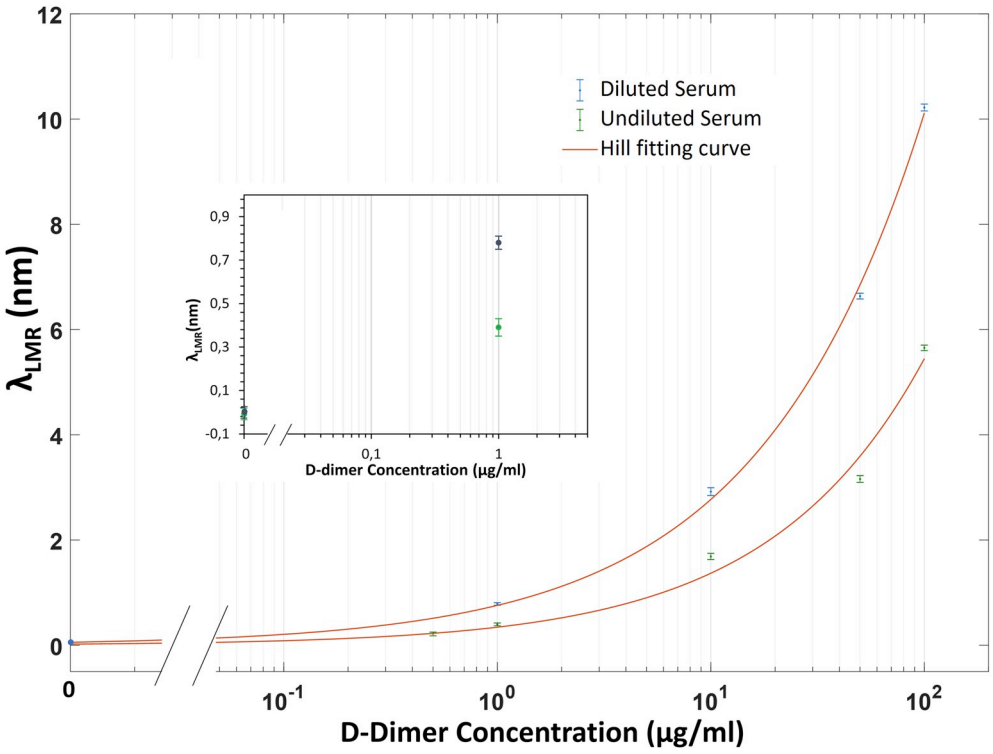

Fig. 5. Calibration curves obtained in human serum. The calibration curves of two distinct D-shaped fiber biosensors ($n = 1$) detecting D-dimer in human serum are displayed, together with the Hill sigmoidal fitting curves of the experimental points (diluted serum, blue symbols; undiluted serum, green symbols). The inset details the wavelength shift and error bar of the blank and first D-dimer concentrations for both cases.

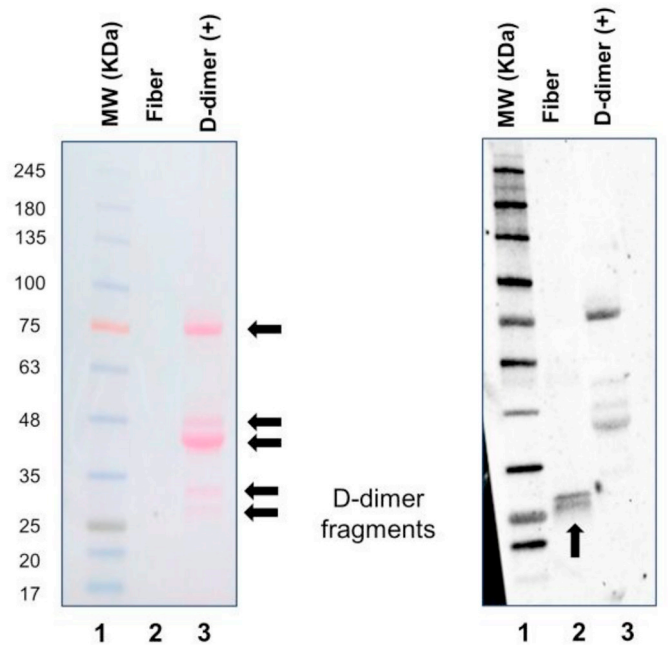

Fig. 6. Detection through Western-blotting of D-dimer protein detached from the functionalized fiber surface. (A) Results of D-dimer separation by SDS-PAGE using the Ponceau staining. The annotation "D-dimer (+)" corresponds to a positive control where human D-dimer protein is analyzed by SDS-PAGE. The black arrows indicate the multiple bands corresponding to D-dimer protein. (B) Results of protein detection through W-b detailing a specific band placed between 25 and 35 kDa (black arrow).

is described in Methods section, while the results are presented in Supplementary Material (Supplementary Table 1 and Supplementary Figs. 4 and 5). By using the previous mentioned workflow, D-dimer fragments corresponding to beta- and gamma-chains of fibrinogen are identified by mass spectrometry, confirming that the D-dimer is covalently bound to the fiber surface.

4. Discussion and conclusions

Due to the pivotal role of D-dimer levels in the cardiovascular area (Weitz et al., 2017), it is obvious that specific and accurate measurement methods are needed. Nowadays, a divergence exists even using similar formats (Riley et al., 2016), making the standardization quite difficult. This discrepancy may be explained by several factors, including employment of monoclonal antibodies with varying specificities and differences in instrumentation used to detect D-dimer.

Here, we report on a LMR-based optical biosensor realized by means of a SnO_{2-x} nanocoated D-shaped fiber for the detection of specific D-dimer/anti-D-dimer interactions, providing a sensitive, simple and label-free biosensing platform for the D-dimer detection. The operating principle consists of binding of a protein (D-dimer) to an antibody (anti-D-dimer) grafted on the D-shaped fiber, which induces changes both in the thickness of the sensitive layer and in the effective RI of the layer itself. Hence, an accurate determination of this change can be attained by detecting the shift of the LMR wavelength, which allows monitoring the binding kinetics by a real-time recording of the optical spectrum. This feature is combined with the unique and peculiar properties of optical fibers: small size, immunity to electromagnetic and radio-frequency interferences, capability to be used in harsh environments, for remote sensing and within multiplexed sensing schemes, and, most importantly, light management.

In this case, D-dimer binding is specific in the presence of not specific proteins (i.e. CRP), and in the presence of human serum, a highly complex biological matrix constituted by more than 10,000 different kinds of proteins (Nanjappa et al., 2014). The response time of the biosensor, roughly 10–20 min, can be considered comparable with other fiber-based biosensing platforms (Chiavaioli et al., 2017a), taking into account that the measurements have been carried out in complex matrices. Interestingly, an outstanding LOD of a 10 ng/mL (in buffer matrix) and 100 ng/mL (in human serum) has been obtained. In addition, it is important to note that the sensitivity of the device may be increased by selecting an overlay material with a higher RI than SnO_{2-x}, which should allow improving the LOD (Del Villar et al., 2012). Nevertheless, the LOD obtained in human serum is below the clinical cutoff value of 500 ng/mL indicated both for plasma and for serum (Linkins and Takach Lapner, 2017; Marill, 2008; Weitz et al., 2017) (a higher level is indicated in (Tan et al., 2017)), which is a key advance towards theranostic treatments of VTE for personalized medicine.

While configurations reported up to now are rather complex with time-consuming methods, such as ELISA tests or fluorescence-based techniques, our label-free approach greatly simplifies the measurement and the device itself compared to other biosensors realized for D-dimer detection (Bernard et al., 2010; Bourigua et al., 2010; Di Nisio et al., 2007; Rowe et al., 1998; Shimony et al., 2011). Clearly, commercially available ELISA kits or other labelled-based techniques can attain comparable or sometimes better results with all the typical drawbacks of such approaches, like sample manipulation and so on. Moreover, the main novelty of the device presented here is the ability to monitor in real time every step of the process, by recording the evolution of the central wavelength of the optical resonance generated with the thin-film deposited on a special D-shaped fiber.

On the other hand, proteomics is considered one of the ideal platforms for biomarker characterization and translation (Geyer et al., 2017). In particular, mass spectrometry is widely used to precisely identify proteins from complex mixtures (Aebersold and Mann, 2016), matching a list of experimental peptide masses with the calculated list of all peptide masses of each protein in a database (Aebersold and Mann, 2003). However, the application of mass spectrometry based proteomics in biosensing design is scarce. For this purpose, a pipeline has been stablished consisting of: i) protein detachment from the fiber surface, ii) immunodetection, iii) protein digestion and subsequent peptide cleaning, iv) mass spectrometry-based proteomics, and v) bioinformatics. This bottom-up workflow has allowed us to unequivocally verify the attachment of D-dimer to the fiber surface and to demonstrate the ability of the technology platform to specifically (>90%) recognize D-dimer and its reliability. Despite further developments are needed to the implementation of the proposed device for clinical applications, this straightforward approach potentially represents a paradigm shift in the development of a fast, simple, high-specificity and label-free biosensing platform, which can be applied to speed up diagnostic healthcare processes of VTE toward an early diagnostic and personalized treatment system.

Declaration of competing interest

The authors declare that they have no known competing financial interests or personal relationships that could have appeared to influence the work reported in this paper.

Acknowledgements

This work is funded by grants from the Spanish Agencia Estatal de Investigación (AEI) and European Regional Development Fund (FEDER) (TEC2016-78047-R) and the Department of Economic Development from Government of Navarra (REF. PC023-24-25, PC081-082, and PI031). The Proteomics Unit of Navarrabiomed is a member of Proteored, PRB3-ISCIII, and is supported by grant PT17/0019/009, of the PE I+D+I 2013–2016 funded by ISCIII and FEDER. This work is partly funded by the European Commission, Directorate-General Communications Networks, Content and Technology (DG CONNECT)

under the ERA-NET Cofund scheme - Horizon 2020 “Horizon 2020 – the Framework Programme for Research and Innovation (2014–2020)” for the project OPTIMO and by National Research Council of Italy (CNR) within the Short Term Mobility program (STM 2017).

Appendix A. Supplementary data

Supplementary data to this article can be found online at https://doi.org/10.1016/j.biosx.2019.100026.

References

Adam, S.S., Key, N.S., Greenberg, C.S., 2009. Blood 113.
Aebersold, R., Mann, M., 2003. Nature 422, 198–207.
Aebersold, R., Mann, M., 2016. Nature 537, 347–355.
Andreev, A., Pantchev, B., Danesh, P., Zafirova, B., Karakoleva, E., Vlaikova, E., Alipieva, E., 2005. Sens. Actuators B Chem. 106, 484–488.
Andreev, A.T., Zafirova, B.S., Karakoleva, E.I., Dikovska, A.O., Atanasov, P.A., 2008. J. Opt. A Pure Appl. Opt. 10, 035303.
Arregui, F.J., Del Villar, I., Zamarreño, C.R., Zubiate, P., Matias, I.R., 2016. Sens. Actuators B Chem. 232.
Bernard, T.J., Fenton, L.Z., Apkon, S.D., Boada, R., Wilkening, G.N., Wilkinson, C.C., Soep, J.B., Miyamoto, S.D., Tripputi, M., Armstrong-Wells, J., Benke, T.A., Manco-Johnson, M.J., Goldenberg, N.A., 2010. J. Pediatr. 156, 651–656.
Bourigua, S., Hnaien, M., Bessueille, F., Lagarde, F., Dzyadevych, S., Maaref, A., Bausells, J., Errachid, A., Renault, N.J., 2010. Biosens. Bioelectron. 26, 1278–1282.
Caucheteur, C., Guo, T., Liu, F., Guan, B.-O., Albert, J., 2016. Nat. Commun. 7, 13371.
Chebil, S., Hafaiedh, I., Sauriat-Dorizon, H., Jaffrezic-Renault, N., Errachid, A., Ali, Z., Korri-Youssoufi, H., 2010. Biosens. Bioelectron. 26, 736–742.
Chiavaioli, F., Baldini, F., Tombelli, S., Trono, C., Giannetti, A., 2017a. Nanophotonics 6, 663–679.
Chiavaioli, F., Biswas, P., Trono, C., Bandyopadhyay, S., Giannetti, A., Tombelli, S., Basumallick, N., Dasgupta, K., Baldini, F., 2014. Biosens. Bioelectron. 60, 305–310.
Chiavaioli, F., Gouveia, C.A.J., Jorge, P.A.S., Baldini, F., 2017b. Biosensors 7 (2), 23.
Chiavaioli, F., Zubiate, P., Del Villar, I., Zamarreño, C.R., Giannetti, A., Tombelli, S., Trono, C., Arregui, F.J., Matias, I.R., Baldini, F., 2018. ACS Sens. 3, 936–943.
Cusano, A., Iadicicco, A., Pilla, P., Contessa, L., Campopiano, S., Cutolo, A., Giordano, M., 2006. Opt. Express 14 (1), 19–34.
Del Villar, Ignacio, Matías, Ignacio R., Arregui, Francisco J., Lalanne, Philippe, 2005. Optimization of sensitivity in Long Period Fiber Gratings with overlay deposition. Opt. Express 13 (1), 56–69.
Gao, Y.Z., Zhang, L., Huo, W.S., Shi, S., Lian, J., Gao, Y.H., 2015. Chin. J. Anal. Chem. 43, 802–807.
Gesztelyi, R., Zsuga, J., Kemeny-Beke, A., Varga, B., Juhasz, B., Tosaki, A., 2012. Arch. Hist. Exact Sci. 66, 427–438.
Geyer, P.E., Holdt, L.M., Teupser, D., Mann, M., 2017. Mol. Syst. Biol. 13, 942.
Gramotnev, D.K., Bozhevolnyi, S.I., 2010. Nat. Photonics 4, 83–91.
Grant, S.A., Glass, R.S., 1999. IEEE Trans. Biomed. Eng. 46, 1207–1211.
Hoa, X.D., Kirk, A.G., Tabrizian, M., 2007. Biosens. Bioelectron. 23, 151–160.
Homola, J., 2008. Chem. Rev. 108, 462–493.
Kikkert, W.J., Claessen, B.E., Stone, G.W., Mehran, R., Witzenbichler, B., Brodie, B.R., Wöhrle, J., Witkowski, A., Guagliumi, G., Zmudka, K., Henriques, J.P.S., Tijssen, J.G.P., Sanidas, E.A., Chantziara, V., Xu, K., Dangas, G.D., 2014. J. Thromb. Thrombolysis 37, 155–164.
Kogan, A.E., Mukharyamova, K.S., Bereznikova, A.V., Filatov, V.L., Koshkina, E.V., Bloshchitsyna, M.N., Katrukha, A.G., Kogan, A.E., 2016. Blood Coagul. Fibrinolysis 27, 542–550.
Kosiel, K., Koba, M., Masiewicz, M., Śmietana, M., 2018. Opt. Laser. Technol. 102, 213–221.
Koukouvinos, G., Petrou, P., Misiakos, K., Drygiannakis, D., Raptis, I., Stefanitsis, G., Martini, S., Nikita, D., Goustouridis, D., Moser, I., Jobst, G., Kakabakos, S., 2016. Biosens. Bioelectron. 84, 89–96.
Lachén-Montes, M., González-Morales, A., Zelaya, M.V., Pérez-Valderrama, E., Ausín, K., Ferrer, I., Fernández-Irigoyen, J., Santamaría, E., 2017. Sci. Rep. 7, 9115.
Linkins, L.-A., Takach Lapner, S., 2017. Int. J. Lab. Hematol. 39, 98–103.
Liu, T., Liang, L.-L., Xiao, P., Sun, L.-P., Huang, Y.-Y., Ran, Y., Jin, L., Guan, B.-O., 2018. Biosens. Bioelectron. 100, 155–160.
Longstaff, C., Adcock, D., Olson, J.D., Jennings, I., Kitchen, S., Mutch, N., Meijer, P., Favaloro, E.J., Lippi, G., Thachil, J., 2016. Thromb. Res. 137, 219–220.
Marill, K.A., 2008. J. Emerg. Med. 34, 367–376.
Nanjappa, V., Thomas, J.K., Marimuthu, A., Muthusamy, B., Radhakrishnan, A., Sharma, R., Ahmad Khan, A., Balakrishnan, L., Sahasrabuddhe, N.A., Kumar, S., Jhaveri, B.N., Sheth, K.V., Kumar Khatana, R., Shaw, P.G., Srikanth, S.M., Mathur, P.P., Shankar, S., Nagaraja, D., Christopher, R., Mathivanan, S., Raju, R., Sirdeshmukh, R., Chatterjee, A., Simpson, R.J., Harsha, H.C., Pandey, A., Prasad, T.S.K., 2014. Nucleic Acids Res. 42, D959–D965.
Di Nisio, M., van Es, N., Büller, H.R., 2016. Lancet 388, 3060–3073.
Di Nisio, M., Squizzato, A., Rutjes, A., Büller, H., Zwinderman, A., Bossuyt, P., 2007. J. Thromb. Haemost. 5, 296–304.
Olson, J.D., Cunningham, M.T., Higgins, R.A., Eby, C.S., Brandt, J.T., 2013. Arch. Pathol. Lab Med. 137, 1030–1038.
Ozcariz, A., Dominik, M., Smietana, M., Zamarreño, C.R., Del Villar, I., Arregui, F.J., 2019. Sensors Actuators A Phys 290, 20–27.
Paliwal, N., John, J., 2015. IEEE Sens. J. 15, 5361–5371.
Principe, M., Consales, M., Micco, A., Crescitelli, A., Castaldi, G., Esposito, E., La Ferrara, V., Cutolo, A., Galdi, V., Cusano, A., 2017. Light Sci. Appl. 6 e16226–e16226.
Raskob, G.E., Angchaisuksiri, P., Blanco, A.N., Buller, H., Gallus, A., Hunt, B.J., Hylek, E.M., Kakkar, A., Konstantinides, S.V., McCumber, M., Ozaki, Y., Wendelboe, A., Weitz, J.I., 2014. ISTH steering committee for world thrombosis day. Arterioscler. Thromb. Vasc. Biol. 34, 2363–2371.
Riley, R.S., Gilbert, A.R., Dalton, J.B., Pai, S., McPherson, R.A., 2016. Lab. Med. 47, 90–102.
Rowe, C.A., Bolitho, J.S., Jane, A., Bundesen, P.G., Rylatt, D.B., Eisenberg, P.R., Ligler, F.S., 1998. Thromb. Haemost. 79, 94–98.
Shevchenko, A., Tomas, H., Havli\[sbreve], J., Olsen, J.V., Mann, M., 2007. Nat. Protoc. 1, 2856–2860.
Shimony, A., Filion, K.B., Mottillo, S., Dourian, T., Eisenberg, M.J., 2011. Am. J. Cardiol. 107, 1227–1234.
Shrivastava, A., Gupta, V.B., 2011. Chronicles Young Sci. 2, 21–25.
Socorro, A.B., Santamaria, E., Fernandez-Irigoyen, J., Villar, I. Del, Corres, J.M., Arregui, F.J., Matias, I.R., 2017. IEEE J. Sel. Top. Quantum Electron. 23, 314–321.
Spannagl, M., Haverkate, F., Reinauer, H., Meijer, P., 2005. Blood Coagul. Fibrinolysis 16, 439–443.
Squires, T.M., Messinger, R.J., Manalis, S.R., 2008. Nat. Biotechnol. 26, 417–426.
Stern, L., Desiatov, B., Mazurski, N., Levy, U., 2017. Nat. Commun. 8, 14461.
Tan, X., Chen, G., Liu, Y., Zhou, L., He, L., Liu, D., Liu, Y., Zhang, F., Li, H., Liu, H., 2017. Sci. Rep. 7, 4836.
Tiwari, D., Mullaney, K., Korposh, S., James, S.W., Lee, S.-W., Tatam, R.P., 2017. Sens. Actuators B Chem. 242, 645–652.
Del Villar, I., Zubiate, P., Chiavaioli, F., Urrutia, A., Santano, D., Vicente, A., Giannetti, A., Tombelli, S., Trono, C., Baldini, F., Zamarreño, C.R., Arregui, F.J., 2019;al., February. The nanocoating material: a key element for development of D-shaped fiber-based label-free biosensors. In: Proc. 2nd European Biosensor Symposium 2019, Florence, Italy, February 18-21.
Del Villar, I., Arregui, F.J., Zamarreño, C.R., Corres, J.M., Bariain, C., Goicoechea, J., Elosua, C., Hernaez, M., Rivero, P.J., Socorro, A.B., Urrutia, A., Sanchez, P., Zubiate, P., Lopez, D., De Acha, N., Ascorbe, J., Matias, I.R., 2017. Sens. Actuators B Chem. 240.
Del Villar, I., Hernaez, M., Zamarreño, C.R., Sánchez, P., Fernández-Valdivielso, C., Arregui, F.J., Matias, I.R., 2012. Design rules for lossy mode resonance based sensors. Appl. Opt. 51, 4298–4307.
Weitz, J.I., Fredenburgh, J.C., Eikelboom, J.W., 2017. J. Am. Coll. Cardiol. 70, 2411–2420.
Wu, D.K.C., Kuhlmey, B.T., Eggleton, B.J., 2009. Opt. Lett. 34, 322.
Zhang, B., Kumar, R.B., Dai, H., Feldman, B.J., 2014. Nat. Med. 20, 948–953.
Zubiate, P., Zamarreño, C.R., Del Villar, I., Matias, I.R., Arregui, F.J., 2015. Opt. Express 23, 8045–8050.